

# Predicting vortex merging and ensuing turbulence characteristics in shear layers from initial conditions

Anirban Guha<sup>1</sup> and Mona Rahmani<sup>2</sup>

<sup>1</sup>*Institute of Coastal Research, Helmholtz-Zentrum  
Geesthacht, Geesthacht 21502, Germany.\**

<sup>2</sup>*Department of Mathematics, The University of British Columbia,  
Vancouver, B.C. V6T 1Z2, Canada.*

(Dated: December 16, 2024)

## Abstract

Unstable shear layers in environmental and industrial flows roll up into a series of vortices, which often form complex nonlinear merging patterns like pairs and triplets. These patterns crucially determine the subsequent turbulence, mixing and scalar transport. We show that the late-time, highly nonlinear merging patterns are predictable from the linearized initial state. The initial asymmetry between consecutive wavelengths of the vertical velocity field provides an effective measure of the strength and geometry of vortex merging. The predictions of this measure are substantiated using direct numerical simulations. We also show that this measure has significant implications in determining the route to turbulence and the ensuing turbulence characteristics.

Vortex merging is an important mechanism in the evolution process of a series of adjacent co-rotating vortices [1]. This aesthetically pleasing pattern formation has appealed both artists and scientists, an evidence of the former is the famous painting –*The Starry Night* by the 19<sup>th</sup> century Dutch post-impressionist Vincent van Gogh. Vortex merging commonly occur in shear layers in the oceans [2], terrestrial [3] and planetary atmospheres [4], impinging jets [5], combustible jet flames [6], as well as in less regularly expected areas like the wake of mechanical heart valves [7]. The primary vortices arise from the growth of Kelvin-Helmholtz (KH) instabilities on the interface of two fluids with different streamwise velocities. Through the process of merging, two (or more) neighbouring vortices are advected toward each other and merge into a larger vortex [8]. Vortex merging can significantly enhance the mixing induced by the evolution and turbulent breakdown of KH billows by providing more stirring of the fluids in the two fluid layers [9]. This enhanced mixing has important implications for the estimations of vertical mixing of heat, nutrients and pollutants in the atmosphere, oceans and lakes [10].

In this Letter we show that the complex, *nonlinear* vortex merging patterns are predictable from the *linear initial conditions*. Such merging patterns are illustrated in Fig. 1, where a numerical simulation of a shear layer susceptible to KH instabilities has been initiated with a pure random noise. The asymmetrical structure of the KH billows leads to the merging of neighbouring vortices, albeit in a highly non-uniform way. Similar merging patterns have also been observed in laboratory experiments [11], which indicate the growth of higher subharmonics. Quantitative investigations on the physics of multiple vortex merging and turbulent coherent structures are rare in the literature. Numerical simulations on vortex pairing have revealed that depending on the phase difference (between the primary KH and the first subharmonic component), the outcome in the nonlinear stages can be radically different. The optimal phase difference leads to a “rolling interaction” of vortices, while “shredding interaction” occurs at a non-optimal phase difference [12, 13]. The sensitivity of vortex pairing to phase difference has also been established in laboratory experiments with round jets [14, 15]. This phase difference can be used as a parameter for controlling the transitional behaviour, turbulence structure and mixing in shear layers [16, 17] and round jets [18], and even in noise control applications [19].

We assume the classic vortex-sheet profile of KH instability [20, 21]:  $\bar{u} = U\text{sgn}(z)$  and  $\bar{\rho} = 0.5(\rho_1 + \rho_2) + 0.5(\rho_1 - \rho_2)\text{sgn}(z)$ , where  $\bar{u}$  and  $\bar{\rho}$  respectively denote the streamwise

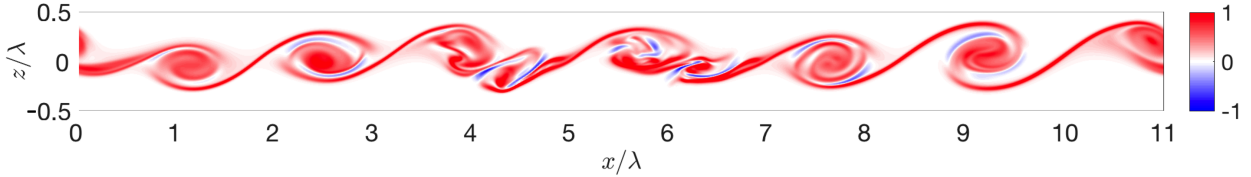


FIG. 1: Irregular vortex merging patterns of 11 wavelengths,  $\lambda = 2\pi/k$ , (of the primary KH) in a density stratified shear layer initially perturbed with random noise (results from a fully 3D DNS). Vorticity contours have been plotted. Negative vorticity primarily ensues from the baroclinic generation.

( $x$ ) background velocity and background density (with  $\rho_2 \geq \rho_1$ ), and  $z$  points vertically upwards. The vortex sheet is perturbed by an infinitesimal sinusoidal disturbance of the form  $\exp[i(kx/\beta + ly - \Omega_\beta t)]$ , where  $k/\beta \in \mathbb{R}^+$  and  $l \in \mathbb{R}^+$  are respectively the streamwise and spanwise wavenumbers, and  $\Omega_\beta \in \mathbb{C}$  is the frequency.

Although the velocities at the interface are not defined, they can be calculated by taking the arithmetic mean of the velocities just above and below. The perturbation vertical velocity at the interface is found from the linearized kinematic condition with  $\bar{u} = 0$ , and is given by  $w_\beta(x, y, 0, t) = -i\Omega_\beta\eta_\beta$ , where  $\eta_\beta$  denotes the interface elevation. This shows that  $w_\beta$  has the same phase as  $\eta_\beta$  provided  $\Omega_\beta$  is purely imaginary (unstable flow with zero phase speed).

The classic dispersion relation for KH instability under the Boussinesq approximation yields:

$$\Omega_\beta \equiv i\gamma_\beta = \pm i\sqrt{\left(U\frac{k}{\beta}\right)^2 - Atg\tilde{k}}, \quad (1)$$

where  $\gamma_\beta$  is the growth rate,  $\tilde{k} = \sqrt{(k/\beta)^2 + l^2}$ ,  $At \equiv (\rho_2 - \rho_1)/(\rho_1 + \rho_2)$  is the Atwood number and  $g$  is gravitational acceleration. Equation (1) shows that for instability,  $\Omega_\beta$  is purely imaginary, hence  $w_\beta$  and  $\eta_\beta$  have the same phase.

For now we restrict ourselves to 2D flows ( $x$ - $z$ ) with polychromatic waves in the streamwise direction (note that now  $l = 0$ );  $k$  is the wavenumber of the primary mode and  $\beta$  is its  $(\beta - 1)$ th subharmonic;  $\beta = 2, 3, \dots$ . Equation (1) shows that the growth rate  $\gamma_\beta$  is inversely proportional to  $\beta$ . Hence the primary mode has the fastest growth rate, and higher the subharmonic, the weaker is its growth rate. We first consider an interface perturbed by a dichromatic disturbance which has modes  $k$  and  $k/\beta$ . Hence the initial disturbance has the

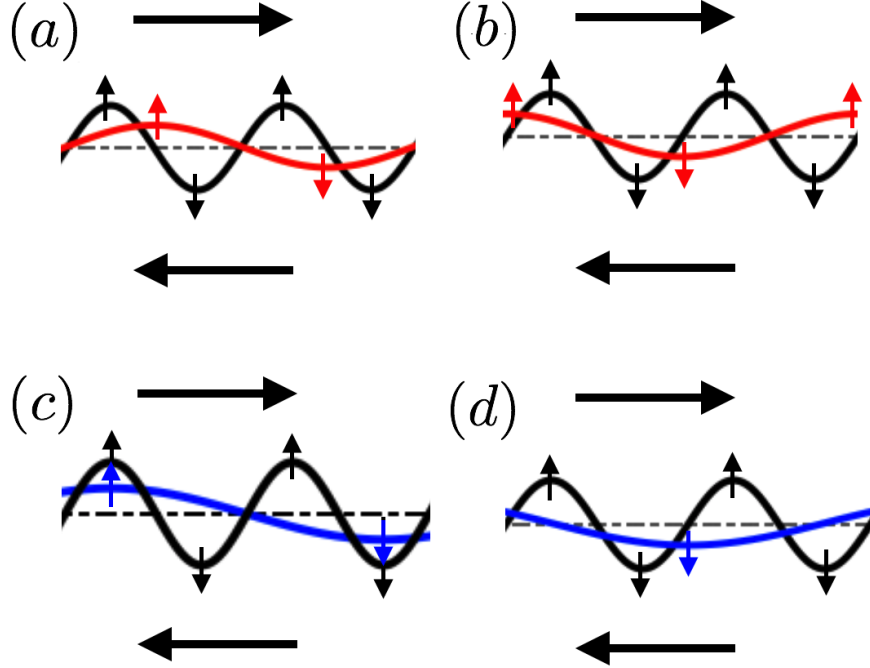


FIG. 2: Schematic showing the first two wavelengths of the primary mode of a KH instability, and its first and second subharmonic modes for different phase shifts. The horizontal (vertical) arrows represent (horizontal) vertical velocity. First subharmonic ( $\beta = 2$ ) for (a)  $\Phi_2 = 0$  (maximum asymmetry), and (b)  $\Phi_2 = \pi/2$  (minimum asymmetry). Second subharmonic ( $\beta = 3$ ) for (c)  $\Phi_3 = \pi/3$  (maximum asymmetry), and (d)  $\Phi_3 = 5\pi/6$  (minimum asymmetry).

form  $\eta(x, 0) = \hat{\eta}_1(0) \sin(kx) + \hat{\eta}_\beta(0) \sin(kx/\beta + \Phi_\beta)$ , where  $\Phi_\beta \in [0, 2\pi)$  denotes the phase difference between the primary and the subharmonic modes. This initial disturbance for a short time would evolve as  $\eta(x, t) = \hat{\eta}_1(0)e^{\gamma_1 t} \sin(kx) + \hat{\eta}_\beta(0)e^{\gamma_\beta t} \sin(kx/\beta + \Phi_\beta)$ . The physical mechanism behind vortex pairing is explained in Fig. 2. In Fig. 2(a), the first subharmonic mode (in red) tends to oppositely displace consecutive wavelengths of the primary mode (in black); the first wavelength (which gives rise to the first KH billow) moves upward while the second (which gives rise to the second KH billow) moves downward. The horizontal velocity shear advects the center of the billows toward each other, leading to pairing. If no asymmetry is introduced by the subharmonic mode, there wouldn't be any pairing; see Fig. 2(b). The only difference between Figs. 2(a)–2(b) is the phase-shift,  $\Phi_2$ . In a very similar manner, the second subharmonic induces pairing in Fig. 2(c) but does not in Fig. 2(d). The basis of the above argument is the fact that the interface elevation of any given mode and the

corresponding vertical velocity are in phase.

Since asymmetry induced by the  $w$  velocity in two neighboring wavelengths of the primary mode leads to merging, we propose a quantitative measure that captures this effect. We consider two consecutive wavelengths of the primary mode and find the integral of the  $w$  velocity in each of them. The integrated  $w$  velocity due to the primary mode will always cancel out, but that due to the subharmonic mode can remain. We define a quantity  $\mathcal{A}$  that measures the strength of the subharmonic mode induced asymmetry with respect to the  $w$  velocity amplitude of the primary mode. Mathematically we write it as follows:

$$\begin{aligned} \mathcal{A}_\beta^{(m,m+1)}(t) &= \frac{\hat{w}_\beta(t)}{\hat{w}_1(t)} \left[ \int_{2(m-1)\pi/k}^{2m\pi/k} \sin\left(\frac{k}{\beta}x + \Phi_\beta\right) dx \right. \\ &\quad \left. - \int_{2m\pi/k}^{2(m+1)\pi/k} \sin\left(\frac{k}{\beta}x + \Phi_\beta\right) dx \right] \\ &= -\frac{4\beta}{k} \frac{\gamma_\beta \hat{\eta}_\beta(0)}{\gamma_1 \hat{\eta}_1(0)} e^{\Delta\gamma t} \sin^2\left(\frac{\pi}{\beta}\right) \cos\left(\frac{2m\pi}{\beta} + \Phi_\beta\right), \end{aligned} \quad (2)$$

where  $\Delta\gamma \equiv \gamma_\beta - \gamma_1$ . The prefix ' $m, m+1$ ' of  $\mathcal{A}_\beta$  signifies that we are comparing the  $m$ -th wavelength with the  $(m+1)$ -th wavelength of the primary mode, where the asymmetry is induced by the  $(\beta-1)$ -th subharmonic. The asymmetry is predicted after time  $t$  based on linear theory. Unless otherwise stated, we will evaluate the asymmetry at the initial time ( $t=0$ ).  $\mathcal{A}_\beta^{(m,m+1)} > 0$  implies that two nearby vortices move towards each other and undergo merging, the higher the magnitude, the quicker (or more energetic) is the merging. Likewise,  $\mathcal{A}_\beta^{(m,m+1)} < 0$  implies that the two neighboring vortices move away from each other. We also note that, although the asymmetry seems directly proportional to  $\beta$  in Eq. (2), it is actually the opposite, which can be quickly verified from the terms  $\gamma_\beta/\gamma_1$  and  $\sin^2(\pi/\beta)$ .

The phases leading to the maximum and minimum magnitudes of  $\mathcal{A}_\beta^{(m,m+1)}$  are

$$\begin{aligned} \Phi_\beta^{max} &= m\pi \left(1 - \frac{2}{\beta}\right) \text{ and } \pi \left[1 + m \left(1 - \frac{2}{\beta}\right)\right], \\ \Phi_\beta^{min} &= \pi \left[\frac{1}{2} + m \left(1 - \frac{2}{\beta}\right)\right] \text{ and } \pi \left[\frac{3}{2} + m \left(1 - \frac{2}{\beta}\right)\right]. \end{aligned}$$

Let us assume that the interface is initially perturbed with the primary disturbance and its first and second subharmonics:

$$\eta(x, 0) = \hat{\eta}_1(0) \sin(kx) + \sum_{\beta=2}^3 \hat{\eta}_\beta(0) \sin\left(\frac{k}{\beta}x + \Phi_\beta\right). \quad (3)$$

Here 6 consecutive wavelengths of the primary wavelength need to be considered for observing the pairing pattern (which would repeat after every six wavelengths). We do not consider any higher subharmonics ( $\beta > 3$ ) since the growth-rate of these modes fall rapidly and are therefore of little consequence. We define the total asymmetry between two consecutive wavelengths (of the primary mode) as

$$\mathcal{A}_{total}^{(m,m+1)} = \mathcal{A}_2^{(m,m+1)} + \mathcal{A}_3^{(m,m+1)}.$$

Depending on the phases  $\Phi_2$  and  $\Phi_3$ , the asymmetries induced by these two subharmonics may largely add-up or may largely cancel out. For simplicity, we restrict to unstratified shear flows ( $At = 0$ ). We span the entire  $\Phi_2$ - $\Phi_3$  space to see what combinations of these phase-shifts lead to high or low asymmetry. We also limit our analysis to initial amplitudes satisfying  $(\hat{\eta}_2(0)/\hat{\eta}_1(0))^2 + (\hat{\eta}_3(0)/\hat{\eta}_1(0))^2 = 2$ . In this respect three cases are considered: (i) C1:  $\hat{\eta}_2(0)/\hat{\eta}_1(0) = 1.41$  and  $\hat{\eta}_3(0)/\hat{\eta}_1(0) = 0.11$ , (ii) C2:  $\hat{\eta}_2(0)/\hat{\eta}_1(0) = 1$  and  $\hat{\eta}_3(0)/\hat{\eta}_1(0) = 1$ , and (iii) C3:  $\hat{\eta}_2(0)/\hat{\eta}_1(0) = 0.11$  and  $\hat{\eta}_3(0)/\hat{\eta}_1(0) = 1.41$ . Furthermore, since asymmetry depends on the wavelength-pair ' $m, m + 1$ ', we consider the maximum absolute asymmetry, i.e.  $\max(|A_{total}|)$  among all ' $m, m + 1$ ' pairs, and plot it in Fig. 3. We observe that when the first subharmonic is very strong (Fig. 3(a)),  $\max(|A_{total}|)$  is nearly independent of  $\Phi_3$ ; the asymmetry is nearly determined by  $\Phi_2$ . However, increasing the relative strength of the second subharmonic increases the uniformity of  $\max(|A_{total}|)$  in the  $\Phi_2$ - $\Phi_3$  space, as is clearly observed in Fig. 3(c). Hence a strong second subharmonic always yields moderate asymmetry independent of the phases.

While the above analysis revealed the importance of initial phase differences and amplitude ratios in deciding the 'global' picture of asymmetry (using  $\max(|A_{total}|)$ ), the 'local' asymmetry  $\mathcal{A}_{total}^{(m,m+1)}$  is the key in providing quantitative estimates of the propensity towards vortex merging. To this end we keep  $\hat{\eta}_2(0)/\hat{\eta}_1(0) = 1$  and  $\hat{\eta}_3(0)/\hat{\eta}_1(0) = 1$ , and vary the initial phase differences: (i)  $\Phi_2 = 0$  and  $\Phi_3 = \pi$ , (ii)  $\Phi_2 = \pi/2$  and  $\Phi_3 = 0$ , and (iii)  $\Phi_2 = \pi/2$  and  $\Phi_3 = \pi/2$ . These cases will be hereafter labelled as S1, S2 and S3. The value of  $\max(|A_{total}|)$  is 7 for S1, which is more than twice of the values corresponding to S2 ( $\max(|A_{total}|) = 3$ ) and S3 ( $\max(|A_{total}|) = 2.6$ ). Fig. 4(a) corresponds to S1, and shows a moderately positive  $\mathcal{A}_{total}^{(1,2)}$  and  $\mathcal{A}_{total}^{(5,6)}$ , a strongly positive  $\mathcal{A}_{total}^{(3,4)}$ , a strongly negative  $\mathcal{A}_{total}^{(2,3)}$  and  $\mathcal{A}_{total}^{(4,5)}$ , and a weakly negative  $\mathcal{A}_{total}^{(6,1)}$ . This implies vortices 1-2 and 5-6 will slowly pair, while the pairing of 3-4 would be far rapid. Both 2-3 and 4-5 will move away from each other.

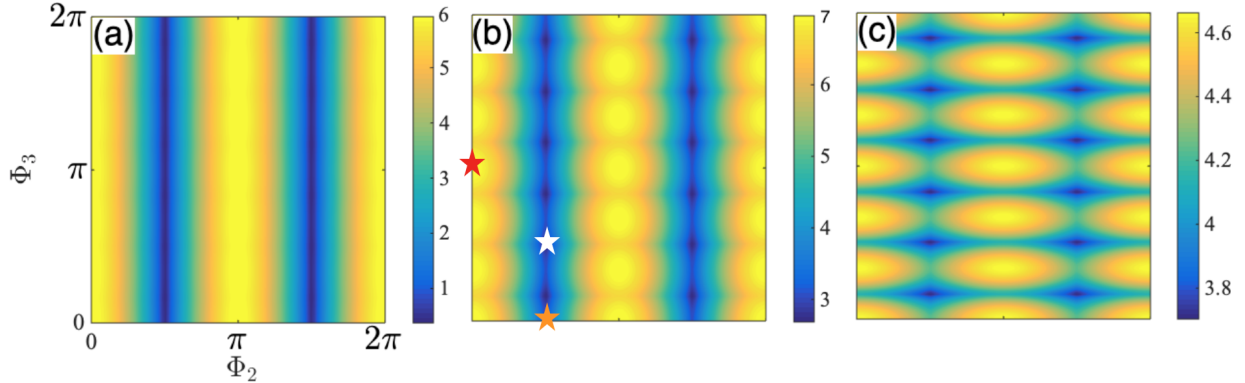


FIG. 3: Maximum absolute asymmetry  $\max(|A_{total}|)$  out of 6 consecutive wavelength pairs in an unstratified KH instability. The entire initial phase-shift space ( $\Phi_2$ – $\Phi_3$ ) is spanned. Results are shown for the following amplitude ratios: (a) Case C1, (b) Case C2, and (c) Case C3. Each sub-figure has its own colorbar. Red, orange and white stars respectively denote cases S1, S2 and S3.

While Fig. 4(a) has alternative positive and negative asymmetries (meaning the maximum extent of merging is *pairing*), Fig. 4(b) reveals a different picture – both 1–2 and 2–3 have positive asymmetries, while 3–4 has a negative one. This indicates the formation of *triplets*. Fig. 4(c) indicates zero asymmetry for vortices 3–4 and 6–1, and are preceded by a negative asymmetry. This indicates that vortices 3 and 6 wouldn't undergo pairing. The veracity of all these predictions, made *solely* based on initial amplitude ratios and phase shifts, need to be substantiated using accurate numerical simulations.

Coherent structures appearing in transitional and turbulent shear flows can be accurately simulated using direct numerical simulations (DNS). To this end, we perform simulations using modest Reynolds number ( $Re = 2000$ , where  $Re \equiv \Delta U h_0 / \nu$ ;  $\nu$  is the kinematic viscosity,  $\Delta U$  and  $h_0$  are respectively the shear velocity and length scales) DNS, that are more realizable in laboratory and/or industrial settings. The shear layer is initially assumed to be represented by  $\bar{u} = \tanh(z)$ ; the velocity and the vertical coordinate  $z$  are respectively non-dimensionalized by  $\Delta U/2$  and  $h_0/2$ . The governing 3D incompressible, non-dimensional Navier-Stokes equations are solved using a pseudo-spectral code, see Refs. [22, 23]. We keep the respective  $x$ ,  $y$  and  $z$  dimensions as  $(L_x, L_y, L_z) = (6\lambda_{KH}, 0.8\lambda_{KH}, 3\lambda_{KH})$ , where  $\lambda_{KH}$  denotes the wavelength of the most unstable KH mode. The boundary conditions are periodic in both  $x$  and  $y$  directions and free slip at  $z = 0$  and  $z = L_z$ . The number

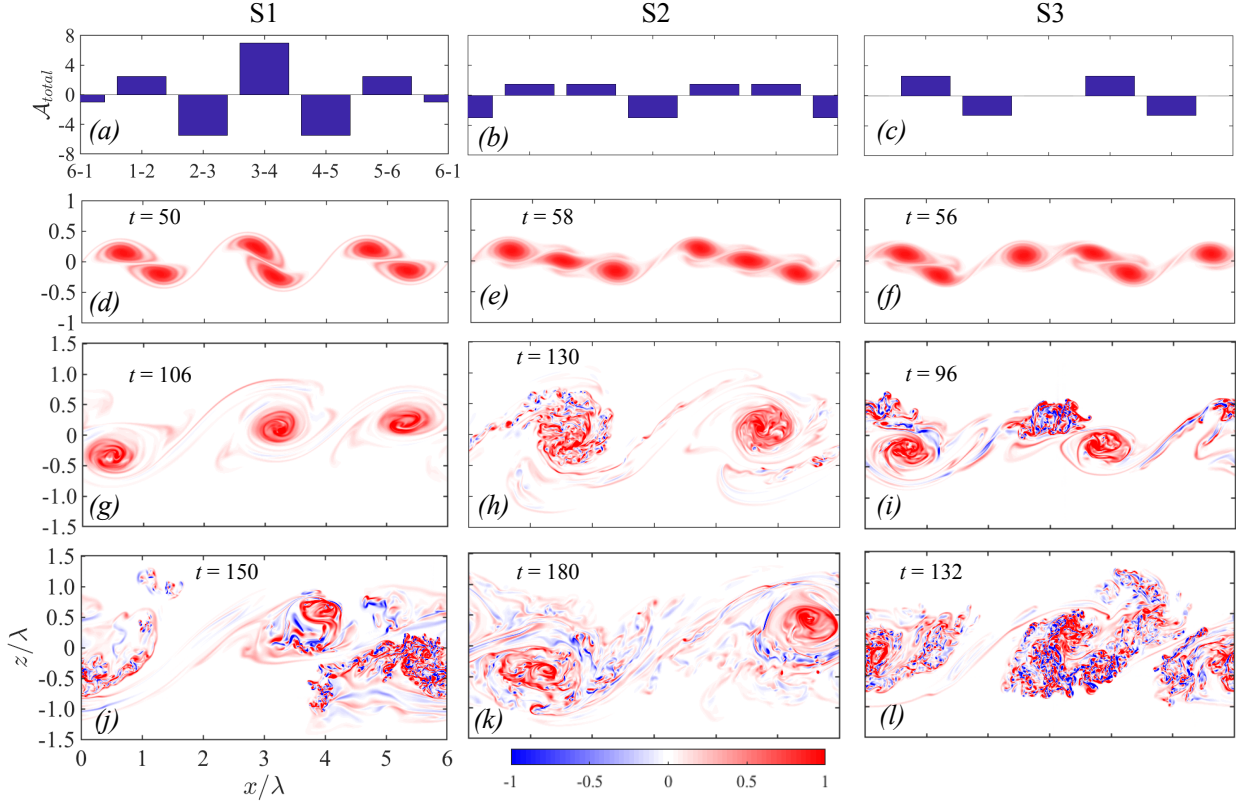


FIG. 4: (a)-(c): Total asymmetry between consecutive wavelengths in an unstratified KH instability. (d)-(f) Nonlinear evolution of KH instability using DNS during the first merging event. (g)-(i) Transition to turbulence in merged KH billows before the second merging event. (j)-(l) Turbulent phase of KH billows just before the last merging event. (a,d,g,j) Case S1, (b,e,h,k) Case S2, and (c,f,i,l) Case S3. The time  $t$  is non-dimensionalized by  $h_0/\Delta U$ .

of mesh points used are:  $(N_x, N_y, N_z) = (1152, 160, 576)$ , which resolves the Kolmogorov length scale.

The DNS results for the cases S1–S3 during the first merging event are respectively shown in Figs. 4(d)–4(f). We find that the observed merging patterns are exactly as predicted by  $\mathcal{A}_{total}^{(m,m+1)}$ , shown in Figs. 4(a)–4(c). The phase relations between the primary mode and its subharmonics also have significant implications for the nonlinear evolution of the vortices in later stages and their turbulent breakdown, as shown in Figs. 4(g)–4(i) and 4(j)–4(l). In case S1, the merged vortices 1-2 and 5-6 undergo a second merging event, see Fig. 4(g). The merging of vortices 3-4 into a single vortex is underway in Fig. 4(j). The development of small-scale structures is delayed until the last merging event. For case S2, during the

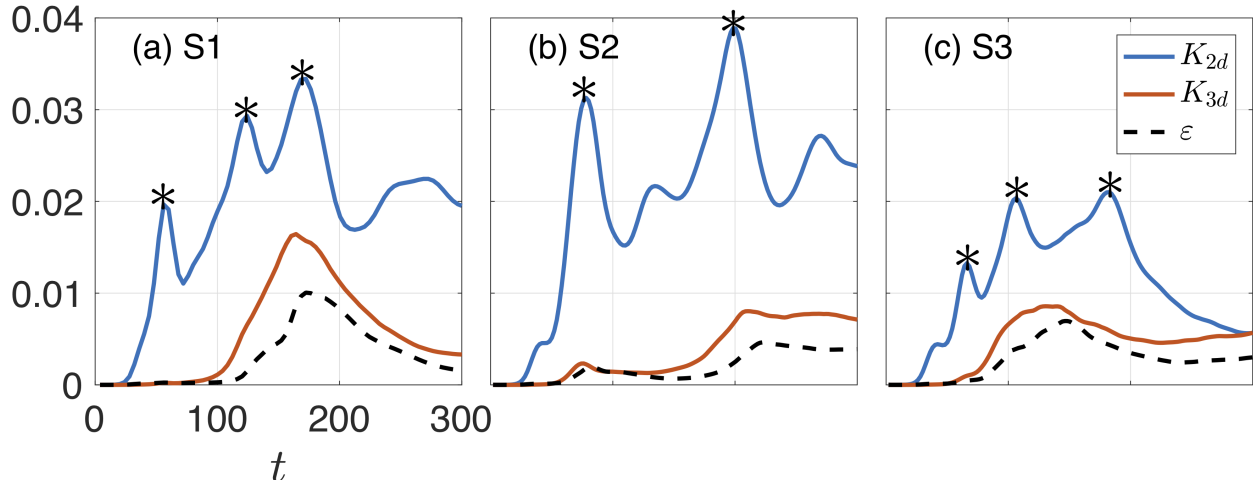


FIG. 5: Time evolution of the dimensionless two- and three-dimensional kinetic energy,  $K_{2d}$  and  $K_{3d}$  and the rate of viscous dissipation of kinetic energy  $\varepsilon$ . The parameter  $\varepsilon$  has been multiplied by a factor of 20 for plotting. The peaks in  $K_{2d}$  corresponding to merging events are marked by stars.

first merging event each three vortices form a triplet. The triplets are fairly symmetric and hence resist pairing for a relatively long time, see Fig. 4(h). Finally they undergo pairing after turbulent-like structures have grown in the cores, see Fig. 4(k). In case S3, the left-out vortices 3 and 6 eventually merge with vortices 4-5 and 1-2, respectively (Fig. 4(i)). This merging event is a “shredding interaction”, and leads to the most vigorous disintegration of the core vortex, see Fig. 4(l).

The growth of turbulent-like coherent structures is a consequence of 3D motions extracting energy from the 2D flow. To quantify the strength of the 2D and 3D motions, and the intensity of turbulence, we utilize the definitions of the 2D kinetic energy:  $K_{2d} = \langle \mathbf{u}_{2d} \cdot \mathbf{u}_{2d} \rangle_{xz}$ , the 3D kinetic energy:  $K_{3d} = \langle \mathbf{u}_{3d} \cdot \mathbf{u}_{3d} \rangle_{xyz}$ , and the rate of viscous dissipation of the total kinetic energy:  $\varepsilon = Re^{-1} \langle (\partial u_i / \partial x_j)^2 \rangle_{xyz}$ , with  $\langle \rangle$  denoting the averages in the specified directions (e.g. see Ref. [24]). In these definitions the velocity field has been partitioned into three parts:  $\bar{\mathbf{u}}(z) = \langle \mathbf{u} \rangle_{xy}$ ,  $\mathbf{u}_{2d}(x, z) = \langle \mathbf{u} \rangle_y - \langle \mathbf{u} \rangle_{xy}$ , and  $\mathbf{u}_{3d}(x, y, z) = \mathbf{u} - \bar{\mathbf{u}} - \mathbf{u}_{2d}$ . The competition between  $K_{2d}$  and  $K_{3d}$ , and the time evolution of  $\varepsilon$ , are shown in Fig. 5 for the cases S1-S3. Note that after the time shown (i.e.  $t > 300$ ) all the motions start to decay. The intensity of the 2D and 3D motions and the viscous dissipation rate varies significantly between the different cases. The highest values in  $K_{2d}$  correspond to the case

S2, where triplets are formed and the vertical extent of the merged vortices are the largest. The major local peaks in  $K_{2d}$  mark the merging events. For example, in cases S1 and S3, three merging events occur, while in the case S2, only two merging events occur. The global maxima in  $K_{3d}$  and  $\varepsilon$  occur close to the last merging event in the cases S1 and S2, and close to second merging in the case S3, where the second merging involves the agglomeration of the most asymmetric vortices. The peaks in  $K_{3d}$  and  $\varepsilon$  are the highest for S1 with the highest  $\max(|A_{total}|)$ . The values of the peaks of  $K_{3d}$  are almost the same for the cases S2 and S3 which have close values of  $\max(|A_{total}|)$ . We therefore conclude that the initial asymmetry of the primary KH wave with respect to its subharmonic modes, given by the global measure  $\max(|A_{total}|)$ , has significant implications for the intensity of the ensuing turbulence. For the highest  $\max(|A_{total}|)$ , vortex merging occurs either earlier (as in S1 compared to S2) or more energetically (as in S1 compared to S3). In the former case, the flow has more time to develop small-scale 3D turbulent motions before the decay starts (e.g. see Ref. [9]) and in the latter case, the 3D motions can extract energy more efficiently from the 2D flow during the active turbulent phase.

In summary, from the initial asymmetry in the vertical velocity field, we derived a useful measure which shows that the highly nonlinear, complex merging patterns and the ensuing turbulence characteristics in shear layers are predictable from the linearized initial state. This also implies that in realistic situations, the route to turbulence, coherent structures and turbulent characteristics are strongly dependent on the initial disturbances. Therefore in future, it may be possible to engineer flows to achieve optimal turbulence and mixing.

A.G. thanks Alexander von Humboldt foundation for funding. The computational resources for this work was provided by Compute Canada.

---

\* Also at Department of Mechanical Engineering, Indian Institute of Technology Kanpur, U.P. 208016, India.; anirbanguha.ubc@gmail.com

- [1] I. M. Lansky, T. M. O’Neil, and D. A. Schecter, Phys. Rev. Lett. **79**, 1479 (1997).
- [2] P. Flament, R. Lumpkin, J. Tournadre, and L. Armi, J. Fluid Mech. **440**, 401 (2001).
- [3] M. S. Buban and C. L. Ziegler, J. Atmos. Sci. **73**, 2061 (2016).
- [4] M.-M. Mac Low and A. P. Ingersoll, Icarus **65**, 353 (1986).

- [5] S. D. Hwang, C. H. Lee, and H. H. Cho, *Int. J. Heat Fluid Fl.* **22**, 293 (2001).
- [6] D. Demare and F. Baillot, *Phys. Fluids* **13**, 2662 (2001).
- [7] D. Bluestein, E. Rambod, and M. Gharib, *J. Biomed. Eng.* **122**, 125 (2000).
- [8] K. B. M. Q. Zaman and A. K. M. F. Hussain, *J. Fluid Mech.* **101**, 449 (1980).
- [9] M. Rahmani, G. A. Lawrence, and B. R. Seymour, *J. Fluid Mech.* **759**, 612 (2014).
- [10] G. N. Ivey, K. B. Winters, and J. R. Koseff, *Annu. Rev. Fluid Mech.* **40** (2008).
- [11] C.-M. Ho and L.-S. Huang, *J. Fluid Mech.* **119**, 443 (1982).
- [12] P. C. Patnaik, F. S. Sherman, and G. M. Corcos, *J. Fluid Mech.* **73**, 215 (1976).
- [13] G. M. Corcos and F. S. Sherman, *J. Fluid Mech.* **139**, 29 (1984).
- [14] G. Broze and A. K. M. F. Hussain, *J. Fluid Mech.* **263**, 93 (1994).
- [15] C. O. Paschereit, I. Wygnanski, and H. E. Fiedler, *J. Fluid Mech.* **283**, 365 (1995).
- [16] M. R. Hajj, R. W. Miksad, and E. J. Powers, *J. Fluid Mech.* **256**, 403 (1993).
- [17] W. Dong, E. W. Tedford, M. Rahmani, and G. A. Lawrence, *Phys. Rev. Fluids* **4**, 063902 (2019).
- [18] S. K. Cho, J. Y. Yoo, and H. Choi, *Exp. Fluids* **25**, 305 (1998).
- [19] J. E. Bridges and A. K. M. F. Hussain, *J. Sound Vib.* **117**, 289 (1987).
- [20] G. K. Batchelor, *An Introduction to Fluid Dynamics* (Cambridge university press, 2000).
- [21] P. G. Drazin and W. H. Reid, *Hydrodynamic stability* (Cambridge university press, 2004).
- [22] K. B. Winters, J. A. MacKinnon, and B. Mills, *J. Atmos. Ocean. Technol.* **21**, 69 (2004).
- [23] W. D. Smyth, J. D. Nash, and J. N. Moum, *J. Phy. Oceanogr.* **35**, 1004 (2005).
- [24] C. P. Caulfield and W. R. Peltier, *J. Fluid Mech.* **413**, 1 (2000).